Discharge and plasma plume characterization of a 100 A-class LaB 6 hollow cathode

S. Mazouffre, R. Joussot, B. Vincent, S. Tsikata

Discharge and plasma plume characterization of a 100 A-class LaB_6 hollow cathode

S. Mazouffre,* R. Joussot, B. Vincent, and S. Tsikata
CNRS, ICARE laboratory, 1c Avenue de la Recherche Scientifique, 45071 Orléans, France
(Dated: September 23, 2021)

This article reports on the characterization of a laboratory model 100 A-class hollow cathode with a sintered lanthanum hexaboride (LaB_6) emitter for high-power Hall thrusters. The cathode has been fired up to 70 A with xenon as working gas. The cathode architecture, test set-up, ignition procedure and power consumption are described first. The second part of this contribution comments on the current-voltage characteristics and the discharge modes obtained for discharge currents in the 30–70 A range and flow rates in the 15–30 sccm range. The cathode operates in spot mode at high discharge currents and in plume mode with large oscillations at low currents and low gas flow rate. Spectral analysis shows that most frequencies resides in the 10–200 kHz range with flat and sharp distributions in plume and spot mode respectively. Finally we present electron temperatures and densities measured in the cathode plasma plume by means of incoherent Thomson scattering. The two quantities decrease along the axis. The density is large (up to $\sim 10^{19}\,\mathrm{m}^{-3}$) and increases with both the ion current and the gas flow rate. The electron temperature increases with the current and decreases with the gas flow rate. The temperature remains relatively low (< 1.5 eV) in spite of large currents and applied powers.

* stephane.mazouffre@cnrs-orleans.fr

I. INTRODUCTION

Hall thrusters are well-established high-efficiency electric propulsion devices used for spacecraft maneuvers [1, 2]. Such thrusters, which rest upon the creation of a low-pressure magnetized plasma discharge in an annular dielectric chamber, feature large thrust-to-power ratios and large thrust densities with specific impulse levels far-above chemical propulsion ones [3, 4]. They are able to operate during long time periods that can exceed 10000 hours, hence a great total impulse in excess of 1 MNs and a velocity increment extent that can accommodate a large variety of space missions [1, 2]. Low-power (< 500 W) and mid-power (0.5–10 kW) Hall thrusters are well suited for orbit transfer, attitude control and station keeping of Cubesats, small satellites and large communication satellites. High-power Hall thrusters operating in the 10 to 100 kW range are now foreseen for applications such as orbit raising of heavy platforms as well as cargo and space tug missions in Earth and Moon orbits [5, 6].

Thermionic hollow cathodes are a critical component for electrostatic propulsion devices as the electron current they emit is required for neutralization of the ion beam generated by the thruster [1]. Moreover, in the case of Hall thrusters, electrons generated by the cathode also play a key role in ion production and plasma discharge sustainment [7, 8]. The hollow cathode technology has greatly evolved and improved over the past decades thanks to advances in material science, manufacture processes and numerical simulations as explained in several articles [8–12]. Available cathodes are stable and efficient, have a long lifespan and are able to operate in a wide range of discharge currents from less than 1 A up to several tens of Amperes.

The cathodes required for maintaining the plasma discharge and for neutralization of the ion beam of large and powerful thrusters have to deliver a current in the 20 A to 300 A range depending on the specific impulse level while consuming several hundreds of Watts of power for heating. Although studies and development of very high current hollow cathodes have started more than a decade ago, there is presently a large amount of works devoted to design optimization, efficiency and reliability improvement and lifetime extension in close relation with on-going projects on high power electric propulsion for deep space missions [13–18]. In this contribution, we present results obtained with a laboratory version of a high-current hollow cathode with a sintered lanthanum hexaboride (LaB_6) insert able to deliver up to 100 A of electron current. Here the cathode has been fired up to 70 A with xenon as working gas. After the description of the cathode architecture and the experimental setup, we show and discuss power consumption, current-voltage characteristic curves, discharge modes and electron properties measured by means of incoherent Thomson scattering instead of a conventional Langmuir probe. The first objective is to compare our observations to the ones realized with other high-current cathodes. The second objective is to examine the impact of the discharge current, the gas flow rate and the mode (plume vs spot) on the electron density and temperature downstream the cathode orifice.

II. CATHODE ARCHITECTURE

A 3D CAD model along with a cross-sectional view of the 100 A-class laboratory model LaB_6 cathode are shown in Fig. 1. The architecture is conventional and shares many common points with existing high-current devices [13–18]. As can be seen in Fig. 1, the cathode consists of two main parts: the base plate and the body that serves as keeper. The total length of the cathode, from the exit orifice to the base rear, is 154 mm. The base that includes electrical connections, gas feeding line and thermal and electrical insulator block is 75 mm in diameter and 40 mm in length. The external body, i.e. the keeper, has an outer diameter of 40 mm and a 114 mm length to accommodate the insert, the heater and heat shields. It is made of graphite. The cathode version used in this study has a 8 mm in diameter cathode orifice from which the plasma expands in the vacuum. The relatively large orifice diameter allows the electric field to penetrate inside the cathode and extract electrons. Electron emission is produced by a 25 mm long and 12 mm inner diameter sintered polycrystalline LaB_6 cylindrical insert, which provides an available emission area of 28.3 cm^2. The work function magnitude has been measured in the 100 °C to 1000 °C temperature range. It has been estimated to 2.7 eV, a value very similar to the ones commonly found in the literature for LaB_6, see e.g. reference [17] and references therein. The LaB_6 emitter is inserted into a thin graphite tube with a 5 mm in diameter aperture to maintain a sufficiently high pressure inside the emitter which facilitates ignition and reduces gas flow rate. Note that graphite has a thermal expansion coefficient similar to the LaB_6 one, a very high melting point (~ 3600 °C), a good electrical conductivity and it does not suffer from boron diffusion. The insert is held in place by a graphite push-piece tube and a tungsten spring placed inside the graphite tube that contains the insert as shown in Fig. 1. The push-piece is sufficiently long and thin to minimize heat conduction from the insert to the base plate. Heating of the LaB_6 emitter is achieved by using a 0.6 mm in diameter tungsten wire axially wrapped around the graphite tube in the emitter region. The heater is electrically insulated with thin Al_2O_3 ceramic that has a maximum operation temperature about 1700 °C. Moreover this ceramic is relatively stable and does not strongly react with the heater and heat shield material, which is necessary to reduce failure probability and reach a long operational life. A tantalum

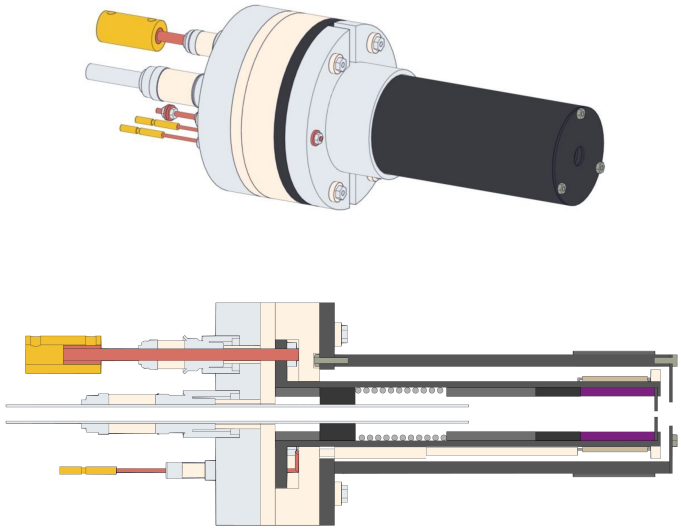

FIG. 1. 3D model of the 100 A cathode developed at ICARE (top) and cross-sectional view showing main elements (bottom).

sleeve that surrounds the heater acts as a thermal shield. The thermal design of the cathode is critical to minimize heat losses and, consequently, the total amount of power required to start and operate the cathode. Therefore proper heat shielding of the cathode heater must warrant low radiative losses. In like manner, material and geometry of the various cathode components must warrant low heat conduction losses. An external igniter electrode has been added to the cathode to ease ignition. The igniter design is based on the one of the 5 A-class cathode studied in our laboratory [19, 20]. The igniter is a 2 mm in diameter tungsten rod placed 2 mm downstream the cathode keeper orifice. The igniter is slightly off-axis to minimize interaction with the expanding cathode plasma. At ignition the voltage is applied to the igniter during about 1 s to trigger electron extraction and switched to the anode afterwards.

III. ASSEMBLY AND CATHODE IGNITION

A. Experimental setup

The cathode has been operated with high-purity xenon in the NExET (New Experiments on Electric Thrusters) vacuum chamber in a standalone configuration [19] at discharge currents up to 70 A, this limit being set by the 3 kW power supply. NExET is a stainless-steel vacuum chamber 1.8 m long and 0.8 m in diameter. For these experiment series the chamber was equipped with a multistage pumping system that was composed of a large dry pump (400 m^3/h), a 350 l/s turbomolecular pump to evacuate light gases and a cryogenic pump with a typical surface temperature of $\sim$ 35 K, which corresponds to about 8000 l/s, to remove gases such as xenon and krypton. A background pressure of 10^{-4} mbar-Xe was achieved with a xenon mass flow rate of 20 sccm. The chamber is equipped with different observation windows, diagnostic ports as well as electrical and gas feed-throughs. The interior of the test bench is easy to access using a large front door.

The anode consists of a water-cooled stainless-steel cylinder 15 cm in diameter and 20 cm long that can handle the high-power discharge. The anode is placed 2 cm in front of the cathode keeper orifice [20]. This configuration produces discharge voltages in the 15 to 25 V range and power up to 1100 W, depending on the current and gas flow rate. The cathode installed in the test setup along with the anode is shown in Fig. 2. Both the cathode and the anode are mounted on rails, as can be seen in the figure, which allows modification of the cathode-to-anode gap. The discharge current and cathode-to-anode voltage were applied with an Elektro-Automatik EA-PSI 9200-70 power supply able to deliver up to 170 A with a maximum output power of 5 kW. The power supply was mostly used in current-limited mode, which allows the voltage to adapt to the discharge need for stable operation. Heating of the LaB_6 emitter prior to ignition was controlled with a high-current low-voltage power supply. Figure 3 is a photograph of the cathode operating with xenon at 30 A and 70 A in plume and spot modes, see section IV. Notice no magnetic field was applied in these investigations.

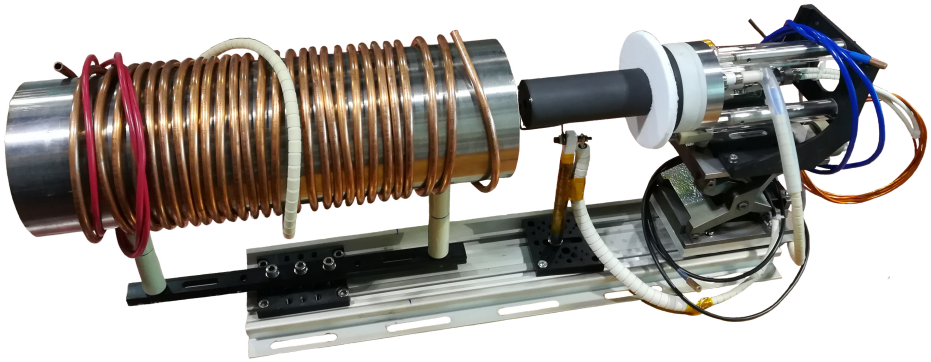

FIG. 2. Cathode test bench showing the cylindrical anode located 2 cm downstream the cathode orifice.

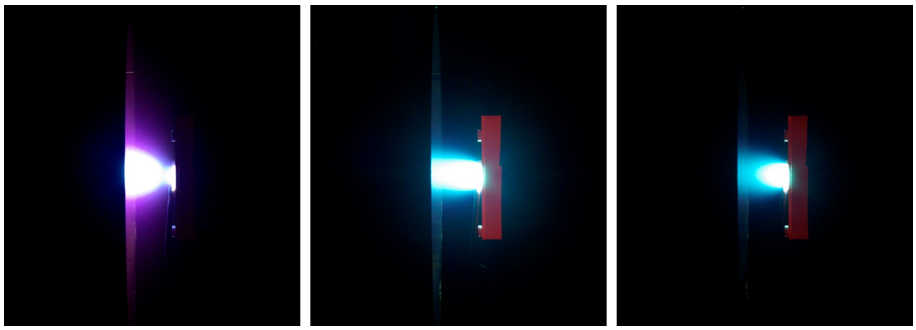

FIG. 3. Photograph of the cathode operating with xenon. From left to right: 30 A and 15 sccm (plume), 70 A and 15 sccm (spot), 70 A and 20 sccm (spot).

B. Ignition

Before starting experiments, the vacuum chamber is typically pumped down to 10^{-6} mbar. The heater current is slowly ramped up to about 25 A (1 A step every minute) before starting the plasma discharge. Ignition typically occurs around 23 A of current, leading to a heating power around 700 W. With the present design, ignition requires about 70 % of the discharge power. Improving thermal insulation to minimize heat losses and optimizing the LaB_6 insert geometry could certainly reduce the needed heating power below 500 W as achieved with other high-current cathodes [15].

When the LaB_6 emitter is sufficiently hot ($I_h \approx 23$ A) the plasma discharge is started in the same manner as with low-power cathodes by injecting the xenon gas through the cathode, applying a relatively large voltage to the igniter electrode and turning on the power supply. Quiet and smooth ignition along with stable discharge with low oscillation level was reached with the following parameters: 30 sccm xenon mass flow rate, anode voltage limited to 200 V, discharge current fixed to 50 A and external igniter electrode voltage and current limited to 400 V and 2 A, respectively. The igniter discharge was power with a Delta Elektronika SM 400-AR-8 (400 V, 4 A) power supplies. The cathode discharge and igniter power supplies are connected in paralell. All power supplies share a common ground. Note that no electrical current flows through the keeper electrode (body) during ignition. After ignition of the cathode discharge, the igniter voltage is switched off. After about 5 minutes, the heater current is quickly decreased to zero. In this work the cathode was always operated with no additional heating, i.e. in self-heating regime. As soon as the heater is turned off the flow rate and current are set to the target value.

The temperature of the cylindrical LaB_6 emitter has been measured by means of electrically insulated type-C thermocouples during the heating phase prior to ignition and during operation for various xenon flow rates and discharge currents [19, 21]. The thermocouples were embedded into the cathode structure and in direct contact with the external surface of the emitter. The temperature was recorded at 3 different axial locations to examine energy deposition inside the emitter. Details about the temperature measurement outcomes can be found in [21]. Only a brief summary is given here. The emitter temperature increases when the discharge current is ramped up as expected. The emitter outer surface temperature is around 1550 K at 23 A and 750 W of heating power. Measurements show a

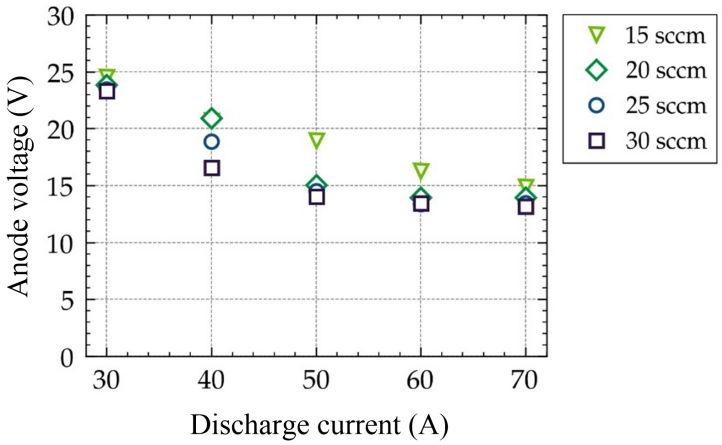

FIG. 4. Current–voltage characteristics for various flow rates.

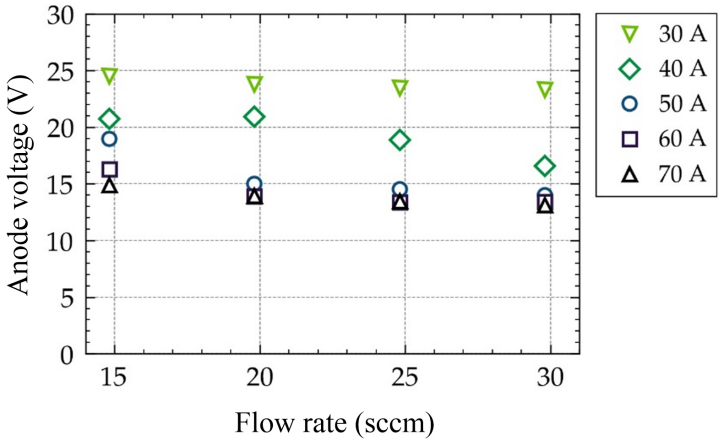

FIG. 5. Anode voltage against flow rate from 30 A to 70 A.

relatively strong temperature gradient in the axial direction. This result indicates the plasma discharge is concentrated in the middle of the insert, as observed in numerical simulations [22].

IV. CURRENT–VOLTAGE CHARACTERISTICS

The discharge current (I_d and anode voltage (V_d) time series have been recorded in steady state by way of a calibrated high-frequency voltage probe (Tektronix P6139A, 500 MHz) and a calibrated Rogowski coil current probe (Stangenes Model 0.5-0.1W,35 MHz, 500 A peak) respectively for xenon flow rates in the 15 sccm to 30 sccm range and current in the 30 A to 70 A range. Notice the mean value of I_d is read on the power supply display. Figure 4 shows voltage–curent characteristics of the 100 A cathode for four different gas flow rates. The evolution of the anode voltage as a function of the flow rate is displayed in Fig. 5 for a discharge current varying from 10 A up to 70 A. The two figures correspond to two different graphic representations of the same data set. They indicate that the discharge power reaches 750 W at 30 A and ∼1 kW at 70 A. As can be seen in Fig.4 and 5, the anode voltage decreases when the current increases and it stays in the [10–25] V range, in agreement with outcomes of preceeding studies [15, 17, 23, 24]. The self-heating regime of hollow cathodes depends on the discharge current magnitude [7]. According to the Richardson-Dushman relation [25], electron current generation is linked to the emitter surface temperature. As low discharge currents provide insufficient heating, the discharge voltage increases to create high kinetic energy ions which maintain the appropriate emitter temperature.

It is by now well-established that the hollow cathode dynamics depends upon the operating conditions and the

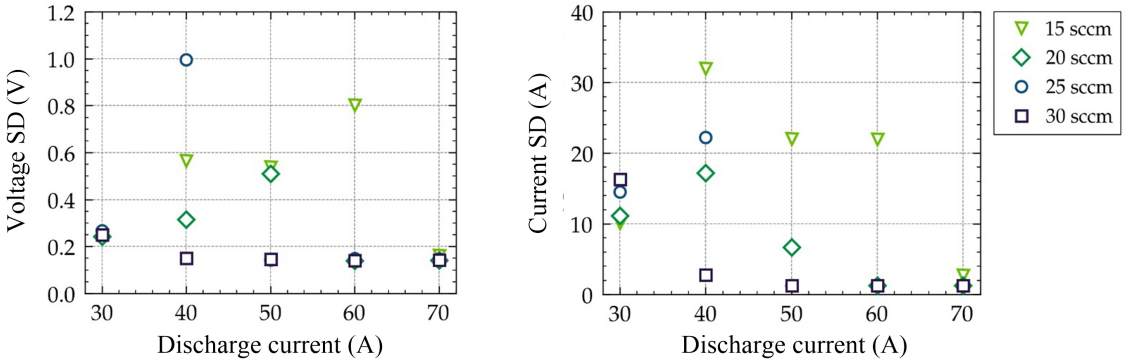

FIG. 6. Voltage (left) and current (right) standard deviation as a function of I_d for various xenon gas flow rate.

geometry [7]. At large mass flow rates, a LaB_6 cathode often operates in the so-called "spot mode" [19, 26]. The plasma forms a spot behind the cathode orifice, as shown in Fig. 3 and voltage and current oscillations remain small. On the contrary, at low mass flow rates and low currents, oscillations are often strong and a plasma plume extends far downstream the orfice. This unstable mode is termed the "plume mode" [19, 26]. In this mode the voltage increases as does the erosion of the cathode front face and keeper. The plume mode is therefore unfavorable as it has negative implications on thruster stability and operational life. A general and simple picture of cathode mode and mode transition cannot be established as many parameters are involved like the flow rate, the gas nature, the current density, the cathode design, the anode geometry [27] and the cathode-to-anode gap [20]. The mode cannot be determined in a reliable manner from a sole visual inspection of the plume, see Fig. 3, or from the current and voltage mean value even though the voltage is often large in plume mode. The proper approach for the determination of the discharge mode rests upon calculation of the current and voltage time series standard deviation, which characterizes the fluctuation level, see [19, 20] and references herein. Large amplitude current fluctuations are indeed associated with the plume mode. More specifically, when the current fluctuation to mean value ratio is below ≈ 0.1 a cathode operates in spot mode according to previous works [19, 28].

Figure 6 shows the voltage and the current standard deviation as a function of the discharge current for a xenon flow rate varying from 15 sccm to 30 sccm. The current standard deviation-to- mean value ratio is plotted in Fig. 7 against the gas flow rate from current in the [30–70] A range. The two figures indicate that the discharge is in spot mode when I_d is larger than 40 A at 25 sccm and when I_d is larger than 30 A at 30 sccm. At 15 sccm, respectively 20 sccm, the discharge operates in spot mode when I_d is larger than 50 A, respectively 70 A. Figure 7 shows oscillations of the current exceeds 40 % of the DC value for low current and low flow conditions. Those results agree with results obtained with other high current cathodes [8, 15, 18]. Figure 7 shows that the cathode discharge is always in spot mode at $I_d = 70$ A whatever the flow rate and always in plume mode at $I_d = 30$ A. Therefore operation in spot mode is possible even at 15 sccm above 70 A. The cathode could however fire in plume mode below this value as transition occurs rapidely when the flow rate is decreased. This is well exemplified in Fig. 6 with the 60 A case for which the spot to plume transition is observed from 20 to 15 sccm. In brief, the cathode operates in plume mode at low mass flow rates and low currents and in spot mode at large flow rates and large currents, in agreement with many works published over a broad range of currents.

Modes and mode transition can be better characterized through the spectral analysis of the discharge current or voltage time series. Figures 8 shows the power spectral density (PSD) of the current traces computed by means of the Fourier transform for the 40 A and the 50 A operating point. The power spectrum greatly depends on the xenon flow rate magnitude. Well-defined peaks with large amplitudes are seen for low flow conditions when the cathode operates in plume mode, which images large current fluctuations.

At 40 A, high amplitude peaks in the PSD can clearly be indentified at 50 kHz and 31 kHz at 15 sccm, respectively 20 sccm. The two peaks at 102 kHz and 62 kHz certainly correspond to the second harmonic. At 25 sccm, the spectrum is more complex with three disctinct peaks at 4.2 kHz, 12 kHz and 42 kHz. The amplitude of the peaks is nevertheless smaller compared with the two previous propellant flow conditions. At 30 sccm, the cathode is considered to operate in spot mode and the power spectrum is broad with no clear peak. Moreover the energy content of the oscillations is very small in that case. The trend is similar at 50 A. A large amplitude peak at 24 kHz with its harmonic can be observed at 15 sccm when the cathode is in plume mode. For the three other flow rates the cathode is in spot mode. Computed spectra are flat and the oscillation energy content is negligible.

PSD have shown that most frequencies resides in the 10–200 kHz range with flat distributions in spot mode and

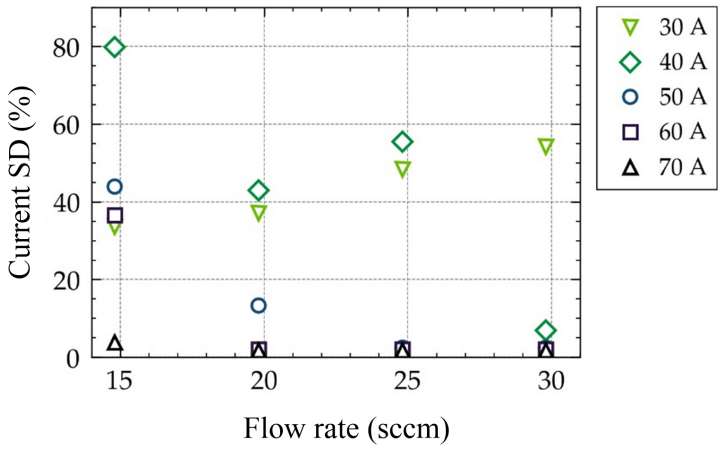

FIG. 7. Discharge current standard deviation in percent against xenon gas flow rate from 30 A to 70 A.

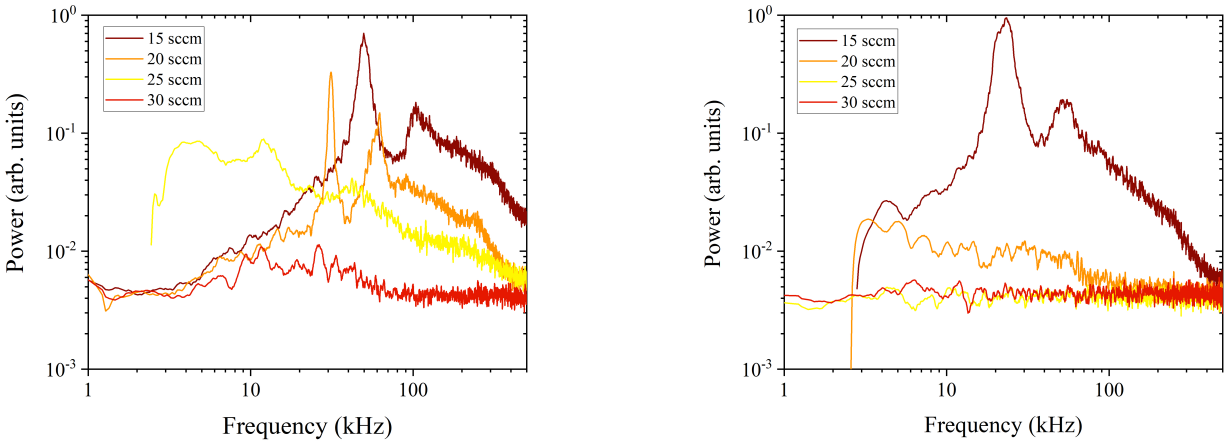

FIG. 8. Power spectral densities obtained from the discrete Fourier transform of the discharge current traces at 40 A (left) and 50 A (right) for 4 values of the xenon flow rate.

sharp peaks in plume mode within the operating domain we explored. This result is in good agreement with previous studies. This frequency range certainly corresponds to a coherent ionization instability as the signature of ion acoustic turbulence (IAT) appears for higher frequencies typically in the 0.5–1 MHz range [29]. As observed in experiments, when an axial magnetic field is applied to a high-current cathode, a rotational mode can couple with the longitudinal mode, yielding a complex plasma motion [30, 31]. The azimuthal mode influences the spot to plume transition [31]. Note that experiments and simulations have demonstrated that at high pressure ($\approx 10^{-4}$ mbar) peaks in the PSD shift towards lower frequencies, which could explain the relatively low frequencies found in this study [29].

V. ELECTRON PROPERTIES IN THE PLUME

Electron temperature and density have been measured downstream the cathode exit plane by means of incoherent Thomson scattering (ITS) instead of electrostatic Langmuir probes in this work. ITS is a non-invasive, direct and spatially-resolved laser-aided diagnostic technique [32–34]. Thomson scattering is the scattering of incident electromagnetic radiation on free electrons, which allows the direct observation of the Electron Energy Distribution Function (EEDF) in the direction of the wave vector $\mathbf{k}$ defined according to the Bragg relation: $\mathbf{k} = \mathbf{k_s} - \mathbf{k_i}$, where $\mathbf{k_s}$ and $\mathbf{k_i}$ are the scattering and incident wave vectors, respectively. Two scattering regimes can be distinguished according to the scattering parameter $\alpha = 1/k\lambda_D$, where λ_D is the Debye length. When $\alpha < 1$ the scattering regime is incoherent:

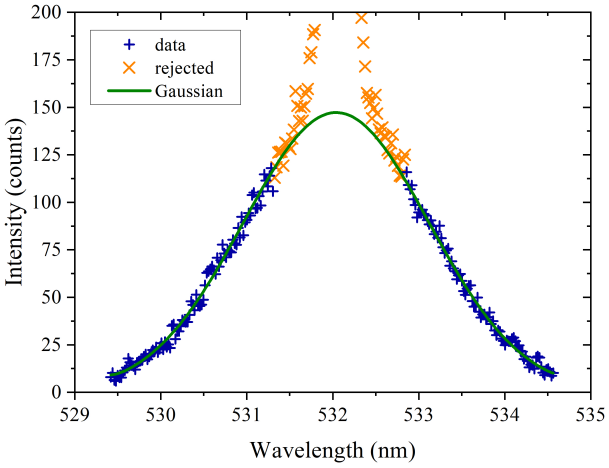

FIG. 9. Thomson scattering spectrum measured at $x = 10\,\text{mm}$ with the cathode operating at 50 A and 30 sccm (350 mJ per laser pulses, average over 6000 pulses).

TABLE I. Cathode parameters, pressure and mode.

Flow rate	I_d	V_d	Power	Pressure	Mode
sccm	A	V	W	mbar	
15	30	22.2	666	1.2×10^{-4}	plume
30	40	14.6	584	1.2×10^{-4}	spot
30	70	15.3	1071	7.8×10^{-5}	spot

the scattering length scales are shorter than the electron screening length. In that case individual electron fluctuations can be observed, allowing electron density and temperature to be determined.

Details about the compact high-sensitivity ITS bench used in this study can be found in reference [34–36]. Only a short description is given here. Coherent light is produced by a 10 Hz Nd:YAG laser (Quantel Q-Smart 850) able to deliver up to 430 mJ per pulse at 532 nm. Several high-reflectivity optics are used to transmit light to the observation volume. Brewster windows mounted at the end of long tubes minimize the stray light level. In the center of the plasma volume, the beam waist is about 0.3 mm. After traversing the plasma, the beam is sent to a beam dump with a large acceptance aperture. Scattered radiation is collected perpendicular to the incident beam direction. A fiber bundle consisting of 45 multi-mode fused silica fibers transfers light from the scattering volume to a spectrometer. A spectrally-narrow, high transmission Volume Bragg Grating notch filter is used to significantly attenuate stray light and Rayleigh-scattered light at 532 nm instead of the usual double- or triple-grating spectrometers with masks. A Princeton Instruments Acton SP-2750 spectrometer fitted with silver-coated mirrors disperses the collected light. The detector is a Princeton Instruments ICCD PI-MAX4: 1024f camera. The combined spectrometer and camera features provide a full wavelength coverage at 532 nm of 5.1 nm and 28.6 nm, respectively, for the 2400 lines mm^{-1} and 600 lines mm^{-1} grating. The ITS diagnostic is calibrated using nitrogen Raman spectra measured at relatively low pressures ($\sim$10 mbar). In this work the optical configuration in terms of k vectors allows the observation of the EEDF in the radial direction.

Figure 9 shows an incoherent Thomson scattering spectrum obtained in the plume of the 100 A-class cathode firing in spot mode at 50 A with 30 sccm xenon flow rate. Acquisition has been performed with a laser pulse energy of 350 mJ and using averaging over 6000 laser shots. As can be seen, stray and Rayleigh light at 532 nm is strongly attenuated. Experimental data points are fitted to a Gaussian function to extract electron properties. The ITS spectrum in Fig. 9 gives values of electron temperature and density of, respectively, 1.1 eV and $7.6 \times 10^{17}\,\text{m}^{-3}$. A detailed systematic uncertainty analysis of the ITS spectra has been conducted in a previous work [36]. It was explained that the two main sources of uncertainties originate from the calibration through the uncertainty on the Raman scattering cross-section and from the Gaussian fitting procedure. In this study the relative uncertainty amounts to about 10 % for n_e and T_e.

ITS spectra have been recorded along the cathode centerline for several discharge conditions: 30 A (15 sccm), 40 A

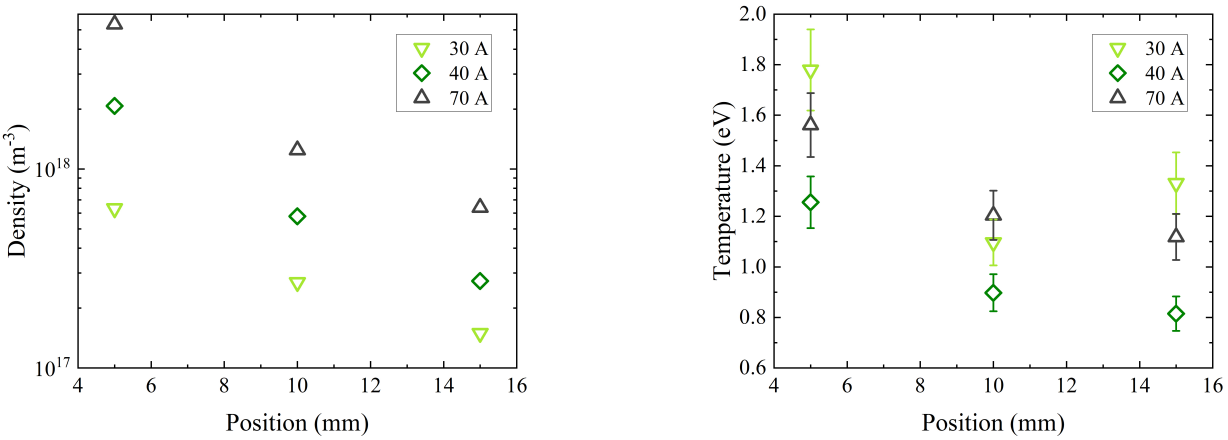

FIG. 10. Electron density (left) and temperature (right) along the cathode centerline at 30 A, 40 A and 70 A. $x = 0$ refers to the cathode keeper orifice. Cathode operating conditions are given in Tab. I.

(30 sccm) and 70 A (30 sccm). Cathode parameters, background pressure in the NExET vacuum chamber and discharge mode are summarized in table I. Figure 10 shows the on-axis development of the electron density n_e and the electron temperature T_e for 30 A, 40 A and 70 A. The position $x = 0$ refers to the cathode keeper orifice exit plane. The cathode-to-anode distance is 2 cm. Note that error bars for n_e are not visible in logarithmic scale. The electron density decreases along the cathode plume centerline in all cases as the cathode plasma expands into vacuum behind the orifice. Similar results have been obtaied in the jet of a 5 A LaB_6 hollow cathode by means of ITS and Langmuir probe [20, 36]. The density decay is steeper at large discharge current: the decrease in n_e reaches almost one order of magnitude at 70 A, whereas n_e drops by a factor of 5 at 30 A. In Fig. 10 one can observe that the electron density drastically increases with the cathode current. At $x = 5$ mm, n_e varies from $\sim 6 \times 10^{17}$ m^{-3} at 30 A to $\sim 5 \times 10^{18}$ m^{-3} at 70 A. Notice that at 70 A, n_e is far above 10^{18} m^{-3} downstream the cathode orifice. The impact of the current and the flow rate upon the electron density is better exemplified in Fig. 11 where I_d is varied from 10 A to 70 A and the gas flow is increased from 15 sccm to 30 sccm. The increase in electron density is here largely due to the higher neutral gas density linked to the higher mass flow rate, which increases the collision frequency and thus the ionization rate. Note that at a given orifice diameter, an increase in the flow rate pushes the density peak value towards the interior of the cathode, which also affects the plume density downstream. The electron current is the main discharge current contribution in a cathode discharge and plume. So the electron density is expected to correlate with the discharge current trend. Experimental data plotted in Fig. 11 indeed shows an increase of n_e with I_d, in agreement with other studies [36]. Interestingly, two regions can be distinguished in the graph according to the slope of the n_e against I_d curve, the frontier being around $I_d \approx 35$ A. The electron density increases faster at large currents. The change in slope in fact marks the transition between the plume mode and the spot mode, see section IV. In spot mode the plasma is more radially constricted, hence a smaller cross-section area of the plasma jet, which is visually observed. The variation of the density against I_d is therefore steeper than in plume mode. The exact values of the electron density and of the slope of the n_e versus I_d curve depends on the oscillations in the plume and the cathode geometry. The induced azimuthal magnetic field can also play an important role in the electron confinement and plume shape at high discharge current. The electron drift velocity was computed at $x = 5$ mm assuming the plume diameter stays constant and equals the keeper orifice diameter (8 mm). Values are 1.3×10^4 m/s, 1.9×10^4 m/s and 4.7×10^4 m/s at 70, 40 and 30 A respectively. The drift velocity is the largest at low current, i.e. in plume mode here where fluctuations are large.

Figure 10 shows the electron temperature decreases along the cathode axis whatever the operating conditions, similarly to what was found experimentally and with computer simulations for a 5 A cathode [36] and for a 25 A cathode [29]. The electron cooling downstream the cathode orifice for all currents originates in energy transfer through collisions and plasma flow expansion [37]. As can be seen in Fig. 10 the highest electron temperature is reached at $x = 5$ mm with a 30 A cathode discharge current and not 70 A as one could expect. This fact is certainly linked to the xenon gas flow rate, which is only 15 sccm at 30 A, as indicated in Tab. I. As the gas density is low, energy transfers are weaker, hence a large temperature. Those experimental results are in agreement with numerical simulations, see e.g. reference [29]. Besides the cathode operates in plume mode at 30 A and 15 sccm. This translates into large voltages and strong oscillations, as shown previously, see Fig. 4–7, which favors electron heating. Figure 11

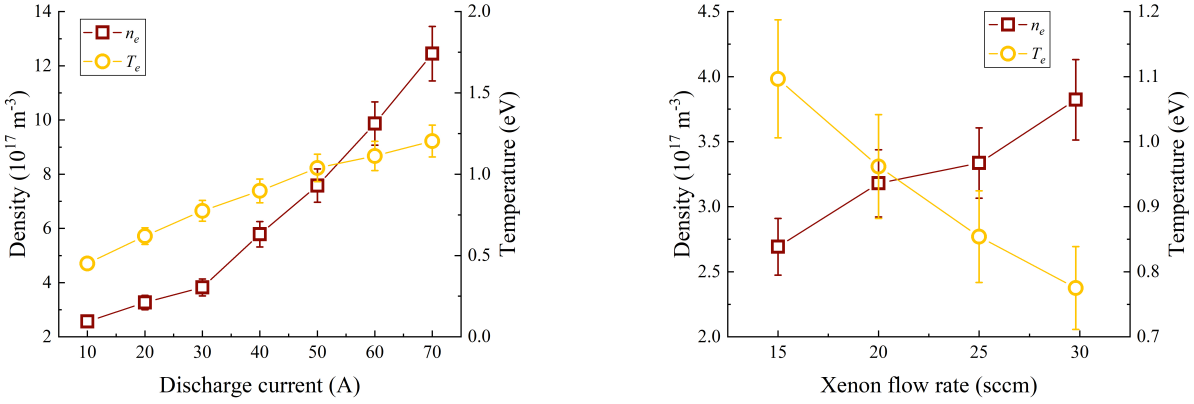

FIG. 11. Evolution of the electron density and temperature with the discharge current (left) and the xenon flow rate (right) at $x = 10$ mm. The flow rate is fixed at 30 sccm for the current series and the current is set at 30 A for the flow rate series.

shows the rate of change of T_e is larger below 40 A, i.e. in plume mode, and the temperature decreases when the flow rate is ramped up for a fixed value of I_d. This last point has two origins: Lessening of energy transfer through collision events and a gradual transition from the plume to the spot mode [29, 36].

As can be seen in Fig. 10 and 11, the electron temperature is surprisingly low, even at high cathode currents. This result is however in agreement with measurements performed with a cylindrical Langmuir probe in the plume of a high current cathode operating at 50 A [38]. Langmuir probe measurements carried out in the plume of a flat disk LaB_6 emitter hollow cathode give for instance an electron temperature around $\sim 3\,eV$ in spot mode at 8 A discharge current with 8 sccm xenon mass flow rate [20, 36], which is larger than what is found here at 70 A. Electrons are heated in the cathode plume largely by joule heating, so the drivers are the resistivity and the electron current density that is mainly determined by the discharge current and the geometry. When comparing the electron temperature for different cathodes, the discharge current might therefore not be the right parameter to consider.

ITS measurements carried out downstream the orifice of the flat disk emitter cathode indicate a temperature between 0.5 eV and 1.5 eV for discharge currents ranging from 2 A to 16 A [34, 36]. Here, the electron temperature does not exeed 2 eV beyond the cathode orifice. Numerical simulations usually give electron temperatures downstream a cathode orifice greater than what is measured by incoherent Thomson scattering, see [29, 36] and references herein. The apparent discrepancy between the ITS and Langmuir probe temperature measurements may originate from numerous factors. An important one is the perturbation of the plasma when an electrostatic probe is inserted and polarized. This is especially relevant close to the cathode orifice where particle fluxes are large. Another possible explanation could be the directional sensitivity of the ITS measurements, as previously suggested [36]. The electron temperature might not be isotropic due to the low collisionality of the plasma outside the cathode. The electron temperatures obtained from ITS here correspond to the temperature along the radial direction, while the values obtained from Langmuir probes and fluid simulations correspond to an average over all the directions. Probing the axial component of the EEDF by ITS was not performed because the arrangement of the vacuum chamber did not permit such a scattering configuration.

VI. CONCLUSION

A laboratory model 100 A-class hollow cathode with a sintered lanthanum hexaboride (LaB_6) emitter has been operated and characterized up to 70 A with xenon. The cathode operates in spot mode at high discharge currents with low current and voltage oscillations whereas it operates in plume mode with large oscillation amplitudes at low currents and low gas flow rate. The cathode is for instance in spot mode at 70 A whatever the flow rate. In contrast it is in plume mode at 30 A even at 30 sccm. PSD of current traces have shown that most frequencies resides in the 10–200 kHz range with flat and sharp distributions in plume and spot mode respectively. This frequency range corresponds to a coherent ionization instability as the signature of ion acoustic turbulence usually appears for higher frequencies.

Electron temperatures and densities have been measured downstream the cathode orifice by means of incoherent Thomson scattering instead of Langmuir probes. Expansion of the plasma from the cathode interior into the vacuum leads to a decay of the two quantities along the axis when moving downstream. Densities are large ($\approx 10^{19}$ m^{-3} at the

cathode outlet at 70 A) and increase with both the ion current and the gas fow rate. A transition in the rate of change of n_e with the current is observed between the plume mode and the spot mode: The rate is larger in spot mode. The electron temperature increases with the current and decreases with the gas flow rate. One relevant factor here is the ionization rate although other parameters like the resistivity, the geometry and the magnetic field certainly play a role. Measured temperatures are relatively low between 0.5 eV and 1.5 eV despite the large current levels. Similar results were obtained by ITS with a 5 A LaB_6 cathode. The difference between the temperatures determined by ITS and the ones given either by electrostatic probes or numerical simulations remains so far unexplained.

ITS measurements at higher discharge currents should be performed to provide additional data about n_e and T_e for comparisons with theoretical models and simulations outcomes. Operating regimes where ion acoustic turbulence is large are certainly of interest. Moreover, investigation of electron properties in cathode plasmas when a static axial magnetic field is applied could bring new insights into the physics and the dynamics of hollow cathodes. Finally, the hypothesis of an anisotropic EEDF in the cathode plasma plume, which could explain the relatively low temperature observed by ITS in the radial direction, must be verified. This task could be accomplished by setting up an optical bench in axial scattering configuration.

ACKNOWLEDGMENTS

This work was financially supported by the CNES Direction des Lanceurs Research and Technology program under grant 161265/00.

DATA AVAILABILITY

Data is available on request from the authors.

[1] S. Mazouffre, "Electric propulsion for satellites and spacecraft: established technologies and novel approaches", *Plasma Sources Sci. Technol.* **25**, 033002 (2016).
[2] I. Levchenko et al, "Perspectives, frontiers and new horizons for plasma-based space electric propulsion", *Phys. Plasmas* **27**, 020601 (2020).
[3] V. V. Zhurin, H. R. Kaufman, R. S. Robinson, "Physics of closed drift thrusters", *Plasma Sources Sci. Technol.* **8**, R1–R20 (1999).
[4] J.-P. Boeuf, "Physics and modeling of Hall thrusters", *J. Appl. Phys.* **121**, 011101 (2017).
[5] J. Brophy, R. Gershman, N. Strange, D. Landau, R. Merrill, T. Kerslake, "300-kW solar electric propulsion system configuration for human exploration of near-earth asteroid", *Proceedings of the 47th Joint Propulsion Conference* (San Diego, CA), AIAA paper 2011-5514 (2011).
[6] S. E. Cusson, M. P. Georgin, H. C. Dragnea, E. T. Dale, V. Dhaliwal, I. D. Boyd, A. D. Gallimore, "On channel interactions in nested Hall thrusters", *J. Appl. Phys.* **123**, 133303 (2018).
[7] D. M. Goebel, I. Katz, *Fundamentals of Electric Propulsion* (Wiley, Hoboken), pp. 243–323 (2008).
[8] D. R. Lev, I. G. Mikellides, D. Pedrini, D. M. Goebel, B. A. Jorns, M. S. McDonald, "Recent progress in research and development of hollow cathodes for electric propulsion", *Rev. Mod. Plasma Phys.*, **3**, 6 (2019).
[9] D. Lev , G. Alon, L. Appel, "Low current heaterless hollow cathode neutralizer for plasma propulsion–Development overview", *Rev. Sci. Instrum.* **90**, 113303 (2019).
[10] D. M. Goebel, R. M. Watkins, K. K. Jameson, "LaB_6 hollow cathodes for ion and Hall thrusters", *J. Propul. Power* **23**, pp. 552–558 (2007).
[11] D. Pedrini, T. Misuri, F. Paganucci, M. Andrenucci, "Development of hollow cathodes for space electric propulsion at Sitael", It Aerospace **4**, 26 (2017).
[12] G. Becatti, R. W.Conversano, D. M. Goebel, "Demonstration of 25,000 ignitions on a proto-flight compact heaterless lanthanum hexaboride hollow cathode", *Acta Astronautica* **178**, pp. 181-191 (2021).
[13] G. Becatti, D. Pedrini, M. M. Saravia, F. Paganucci, T. Andreussi, M. Andrenucci, "5-100 A LaB6 Hollow Cathodes for High-Power Hall Thrusters", *Proceedings of the 36th International Electric Propulsion Conference* (Vienna, Austria), IEPC paper 2019-760 (2019).
[14] D. Pedrini, R. Albertoni, F. Paganucci, M. Andrenucci, "Development of a LaB_6 cathode for high-power Hall thrusters", *Proceedings of the 34th International Electric Propulsion Conference* (Hyogo-Kobe, Japan), IEPC paper 2015-47 (2015).
[15] E. Chu and D. M. Goebel, "High-current lanthanum hexaboride hollow cathode for 10-to-50-kW Hall thrusters", *IEEE Trans. Plasma Sci.* **40**, pp. 2133–2144 (2012).
[16] D. M. Goebel, R. M. Watkins, K. K. Jameson, "LaB_6 hollow cathodes for ion and Hall thrusters", *J. Propul. Power* **23**, pp. 552–558 (2007).

[17] D. M. Goebel and E. Chu, "High-current lanthanum hexaboride hollow cathode for high-power Hall thrusters", *J. Propul. Power* **30**, pp. 35–40 (2014).

[18] D. M. Goebel, G. Becatti, S. Reilly, K. Tilley, S. J. Hall, "High current lanthanum hexaboride hollow cathode for 20-200 kW Hall thrusters", *Proceedings of the 35th International Electric Propulsion Conference* (Atlanta, Georgia), IEPC paper 2017-303 (2017).

[19] R. Joussot, L. Grimaud, S. Mazouffre, "Examination of a 5 A-class cathode with a LaB_6 flat disk emitter in the 2 A–20 A current range" *Vacuum* **146**, pp.52–62 (2017).

[20] G.-C. Potrivitu, R. Joussot, S. Mazouffre, "Anode position influence on discharge modes of a LaB_6 cathode in diode configuration", *Vacuum* **151**, pp. 122–132 (2018).

[21] S. Mazouffre, R. Joussot, B. Vincentz, S. Tsikata, S. Oriol, F. Masson, "Characterization of a 100 A-class LaB_6 hollow cathode for high-power Hall thrusters", Proceedings of the 36th International Electric Propulsion Conference (Vienna, Austria), IEPC paper 2019-776 (2019).

[22] I. G. Mikellides, D. M. Goebel, B. A. Jorns, J. E. Polk, P. Guerrero, "Numerical Simulations of the Partially-ionized Gas in a 100-A LaB_6 Hollow Cathode", *Proceedings of the 33rd International Electric Propulsion Conference* (Washington, D.C.), IEPC Paper 2013-142 (2013).

[23] D. Pedrini, R. Albertoni, F. Paganucci, M. Andrenucci, "Experimental characterization of a lanthanum hexaboride hollow cathode for five-kilowatt-class Hall thrusters", . *J. Propul. Power* **32**, pp. 1557–1561 (2016).

[24] K. Kubota, Y. Oshio, H. Watanabe, S. Cho, Y. Ohkawa, I. Funaki, "Numerical and experimental study on discharge characteristics of high-current hollow cathode", *Proceedings of the 52nd Joint Propulsion Conference* (Salt Lake City, UT), AIAA paper 2016-4628 (2016).

[25] M.E. Kiziroglou, X. Li, A. A. Zhukov, P. A. J. de Groot, C.H. de Groot, "Thermionic field emission at electrodeposited Ni–Si Schottky barriers", *Solid-State Electronics* **52**, pp. 1032-–1038 (2008).

[26] D. M. Goebel, K. K. Jameson, I. Katz, I. G. Mikellides, "Potential fluctuations and energetic ion production in hollow cathode discharges", *Phys. Plasmas* **14**, 103508 (2007).

[27] G.-C. Potrivitu, S. Mazouffre, L. Grimaud, R. Joussot,"Anode geometry influence on LaB_6 cathode discharge characteristics", *Phys. Plasmas* **26**, 113506 (2019).

[28] G. Sary, R. Joussot, L. Grimaud, L. Garrigues, S. Mazouffre, B. Laurent, C. Boniface, S. Oriol, and F. Masson, "Experimental and numerical investigations of a 5 A-class cathode with a LaB_6 flat disk emitter in the 2 A–20 A current range", *Proceedings of the 35th International Electric Propulsion Conference* (Atlanta, GA), IEPC Paper 2017-486 (2017).

[29] I. G. Mikellides, A. Lopez Ortega, D. M. Goebel, G. Becatti, "Dynamics of a hollow cathode discharge in the frequency range of 1–500 kHz", *Plasma Sources Sci. Technol.* **29**, 035003 (2020).

[30] B. A. Jorns, R. R. Hofer, "Plasma oscillations in a 6-kW magnetically shielded Hall thruster", *Phys. Plasmas* **21**, 053512 (2014).

[31] G. Becatti1, D. M. Goebel M. Zuin, "Observation of rotating magnetohydrodynamic modes in the plume of a high-current hollow cathode", *J. Appl. Phys.* **129**, 033304 (2021).

[32] J. Sheffield, D. Froula, S. H. Glenzer, N. C. Luhmann, Jr., *Plasma Scattering of Electromagnetic Radiation – Theory and Measurement Techniques* (Academic Press, Elsevier), 2011.

[33] I. H. Hutchinson, *Principles of Plasma Diagnostics* (Cambridge University Press), pp. 273–321 (2001).

[34] B. Vincent, S Tsikata, S. Mazouffre, T. Minea, J. Fils, "A compact new incoherent Thomson scattering diagnostic for low-temperature plasma studies", *Plasma Sources Sci. Technol.* **27**, 055002 (2018).

[35] B. Vincent, S. Tsikata, S. Mazouffre, "Incoherent Thomson Scattering measurements of electron properties in a conventional and magnetically-shielded Hall thruster", *Plasma Sources Sci. Technol.* **29**, 035015 (2020).

[36] B. Vincent, S. Tsikata, G.-C. Potrivitu, L. Garrigues, G. Sary, S. Mazouffre, "Electron properties of an emissive cathode: analysis with incoherent Thomson scattering, fluid simulations and Langmuir probe measurements", *J. Phys. D: Appl. Phys.* **53**, 415202 (2020).

[37] R. van de Sanden, *The expanding plasma jet : Experiments and model*, PhD thesis, Eindhoven University of Technology, The Netherlands (1991).

[38] R. E. Thomas, H. Kamhawi, G. J. Williams, Jr, "High current hollow cathode plasma plume measurements", *Proceedings of the 33rd International Electric Propulsion Conference* (Washington, DC), IEPC paper 2013-076 (2013).